Proceedings of the 21st ICSMGE, Vienna, Austria, 14 – 19 June 2026. Pistrol, Adam & Schweiger (eds.)
Published by: ÖGG, Austrian Society for Geomechanics, Salzburg, Austria, ISBN 978-3-9503898-4-5
https://doi.org/10.53243/ICSMGE2026-176

Comparative Analysis of Matsuoka-Nakai Criterion and Dilatancy - Effects in Hyperplastic and Hypoplastic Soil Models

Gustav Grimstad
Department of Civil and Environmental Engineering, Norwegian University of Science and Technology, Norway, gustav.grimstad@ntnu.no

Gertraud Medicus
Department of Infrastructure Engineering, University of Innsbruck, Austria, gertraud.medicus@uibk.ac.at

Davood Dadrasajirlou and Seyed Ali Ghoreishian Amiri
Department of Civil and Environmental Engineering, Norwegian University of Science and Technology, Norway

ABSTRACT: This study presents a comparative analysis of hyperplastic and hypoplastic constitutive models for soils, with a focus on their incorporation of the Matsuoka-Nakai failure criterion and the effects of varying dilatancy at different over consolidation ratios (OCRs). The research examines the fundamental differences in the formulation and behavior of these two model types, particularly in their treatment of non-linear soil response and critical state concepts. The hypoplastic model, based on the generalized hypoplastic principles, is evaluated for its ability to capture complex soil behavior without using conventional concepts of elastoplasticity. In contrast, the hyperplastic model, grounded in thermodynamic principles, is assessed for its use of two characteristic constitutive functions: the free energy function and the dissipation function (force potential). The study explores how this formulation incorporates the Matsuoka-Nakai (MN) criterion and accounts for dilatancy in combination with critical state concepts. The research compares the models' stress path predictions and failure states under various loading conditions (Lode angle) and OCR.

KEYWORDS: Soil Modelling, Hyperplasticity, Hypoplasticity, Critical State, Dilatancy

1 INTRODUCTION

A constitutive model for the mechanical behavior of soil connects effective stress and strain. This can for instance be done by connecting the increment in strain (strain rate) to the increment in stress (stress rate). This relation is of "lower order"; hence it is defined as hypo- (lower order) plasticity. In contrast if the effective stress is found from strain through potential functions this is of "higher order"; hence it is defined as hyper- (higher order) plasticity. Independent of the framework used, the goal of a model is to achieve the best prediction of the true material response within the range of interest. And, if the true material response is captured then the model will automatically also fulfill the laws of nature. It is therefore of interest to compare if the response of a hypoplastic model will be quite similar to the response of a hyperplastic model, when modelling the same material.

Critical State Soil Mechanics (Schofield and Wroth, 1968) is widely accepted as a fundamental basis for the development of soil models, independent of the model framework used. In terms of models for clay the common models are, regardless of framework, variants of the Modified Cam Clay Model (MCCM) (Roscoe and Burland, 1968). When the MCCM is combined with Matsuoka-Nakai (MN) (Matsuoka and Nakai, 1974) as in Dadras-Ajirlou et al. (2023) the yield surface has a qualitative agreement with the Asymptotic State Boundary Surface (ASBS) of clay hypoplasticity (Mašín, 2013) in principal stress space.

2 THEORY

2.1 *Hyperplasticity*

Hyperplasticity is defined in Houlsby and Puzrin (2006), even though Wu and Kolymbas (2000) used the thermology hyperplasticity to distinguish elastoplasticity from hypoplasticity, but actually hypoplasticity takes the same role as hypoelasticity does when compared to elasticity (incremental mapping versus total mapping), still none of them are of higher order.

On the other hand, in hyperplasticity the entire constitutive response of a material is expressed through two scalar functions/potentials, the internal/free energy function, u (f, g or h), and force potential, z. Hence, the formulation is at higher order and incremental relationship is derived. The rigidity of the hyperplastic framework ensures that the model follows the second law of thermodynamics and that dissipation is maximized (Ziegler, 1983). From the general form of hyperplasticity a rate dependent model can be defined (hyperviscoplasticity) by having a force potential of higher degree of homogeneity (n) than unity. For the cases with n larger than unity a flow potential, w, is found through a Legendre transformation from z, eq. (1). For cases with $n = 1$, the yield surface, y, is found through a degenerated Legendre transformation.

$$w + z = d = \boldsymbol{\chi} : \dot{\boldsymbol{\varepsilon}}^p \tag{1}$$

Where d is the dissipation, $\boldsymbol{\chi} = \partial z / \partial \dot{\boldsymbol{\varepsilon}}^p$ is the generalized dissipative stress tensor and $\boldsymbol{\varepsilon}^p$ is some internal variable tensor (plastic strain like).

The yield surface of the hyperplastic equivalent of the hyperviscoplastic model given in Dadras-Ajirlou et al. (2023) is retrieved by letting the degree of homogeneity, $n \rightarrow 1$, resulting in eq.(2).

$$y = p'_{eq} - p_0 \tag{2}$$

Where p'_{eq} is the equivalent effective stress measure and p_0 is the isotropic pre-consolidation stress. In true stress space, since in MN-MCCM the generalized dissipative stress and the true effective stress are the same ($\boldsymbol{\chi} = \boldsymbol{\sigma}$) the equivalent effective stress measure is as given by eq. (3). Note that here $\boldsymbol{\sigma}$ is the effective Cauchy stress tensor (where the normally used prime is omitted).

$$p'_{eq} = p'\left(1+\left(\frac{\eta_{SMP}}{M_{SMP}}\right)^2\right) \tag{3}$$

Where η_{SMP} is the ratio of shear stress to normal stress on the Spatial Mobilized Plane (*SMP*) eq. (4), p' is mean effective stress, M_{SMP} controls the critical state line $M_{SMP} = 2 \cdot \sqrt{2/3} \cdot \tan\varphi$. Where φ is the internal critical state friction angle.

$$\eta_{SMP} = \sqrt{p\,\mathrm{tr}\left(\boldsymbol{\sigma}^{-1}\right) - 3} \tag{4}$$

Elasticity follows the Helmholtz free energy function as given by Houlsby et al. (2005), for the case of no plastic part in the free energy and linear stress dependency it gives:

$$\begin{aligned} \dot{\sigma}_{ij} &= \left(\frac{\sigma_{ij}\sigma_{kl}}{\kappa p} + 2g_s p\left(\delta_{ik}\delta_{jl} - \frac{1}{3}\delta_{kl}\delta_{ij}\right)\right)\left(\dot{\varepsilon}_{kl} - \dot{\varepsilon}^p_{kl}\right) \\ \dot{\sigma}_{ij} &= D_{ijkl}\left(\dot{\varepsilon}_{kl} - \dot{\varepsilon}^p_{kl}\right) \end{aligned} \tag{5}$$

Where κ and g_s are the dimensionless elastic bulk compressibility parameter and dimensionless shear stiffness parameter respectively, δ is the Kronecker-delta. For this case $\dot{\boldsymbol{\varepsilon}}^p$ takes the exact role of plastic strain increment.

The pre-consolidation stress follows:

$$p_0 = p_{0ref} \exp\left(\frac{\varepsilon^p_{ii}}{\lambda - \kappa}\right) \tag{6}$$

Which in rate form is:

$$\dot{p}_0 = \frac{p_0}{\lambda - \kappa}\mathrm{tr}\left(\dot{\boldsymbol{\varepsilon}}^p\right) \tag{7}$$

2.2 *Hypoplasticity*

Hypoplasticity is a constitutive framework introduced by Kolymbas (1977), in which elastic and plastic strain is not separated. Hypoplastic models do not include concepts as yield surfaces, plastic potentials, or flow rules. The stress rate $\dot{\boldsymbol{\sigma}}$ is given as a tensor-valued function of the current stress $\boldsymbol{\sigma}$, strain rate $\dot{\boldsymbol{\varepsilon}}$, and void ratio e: $\dot{\boldsymbol{\sigma}} = \boldsymbol{h}(\boldsymbol{\sigma}, \dot{\boldsymbol{\varepsilon}}, e)$. The hypoplastic model for clay (Mašín, 2013, 2014) incorporates concepts from Critical State Soil Mechanics, also though a predefined asymptotic state boundary surface (ASBS). The ASBS is defined using stress normalized by Hvorslev's equivalent pressure p'_e, which is the mean stress on the isotropic normal compression line at the current void ratio. This normalization ensures consistent formulation independent of void ratio scaling. In three-dimensional stress space, critical stress states follow the Matsuoka–Nakai criterion. The critical state line in the p'-e plane is given by:

$$\ln\left(1+e_c\right) = N - \lambda^* \ln\left(2p'/\sigma^*\right) \tag{8}$$

and the isotropic normal compression line (NCL) reads:

$$\ln\left(1+e\right) = N - \lambda^* \ln\left(p'/\sigma^*\right) \tag{9}$$

with σ^* = 1 kPa and material parameters N and λ^*. The full mathematical formulation is given in Mašín (2014), and the calibration procedure is detailed in Kadlíček et al. (2022).

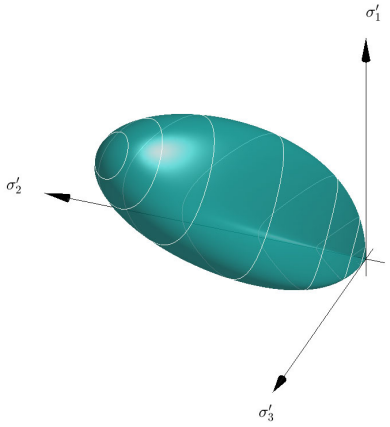

Figure 1. Yield surface for the hyper-MN-MCCM in principal effective stress space

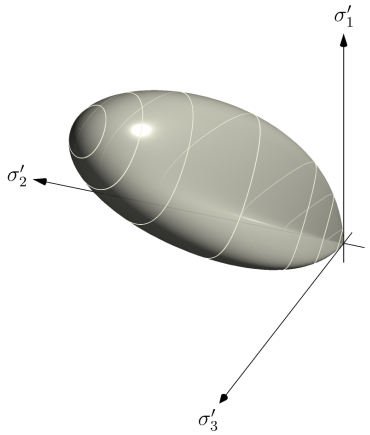

Figure 2. ASBS for clay hypoplasticity in principal effective stress space

2.3 *The yield surface and the ASBS in principal stress space*

Figure 1 shows the yield surface for the Hyper-MN-MCCM in principal stress space with φ = 25.9°, while Figure 2 shows the ASBS for clay hypoplasticity for the same Matsouka-Nakai critical friction angle. In addition, for hypoplasticity, the peak parameter a = 0.30 is set to its default value in all simulations. Qualitatively the two surfaces look to be identical. To further check this the triaxial cross section is plotted. As observed in Figure 3 the p'– q cross section of the yield surface and the ASBS is very similar but not entirely identical.

2.4 *Implementation*

The hyperplastic MN-MCCM is for this study implemented using a modified explicit Euler integration scheme. The formulation is then following the rate dependent form but with n = 1.0010 (close to unity). Eq. (11) gives the flow potential.

$$w = \frac{n-1}{n} r p_0 \left(\frac{p'_{eq}}{p_0}\right)^{\frac{n}{n-1}} \tag{10}$$

Where r is the reference rate, normally implicitly defined by selection of a reference time like one day and calibrated for an oedometer test, but here $r = (n-1)\cdot(\lambda-\kappa)$ is used for simplicity. Subsequently, the plastic strain rate becomes:

$$\dot{\boldsymbol{\varepsilon}}^p = \frac{\partial w}{\partial \boldsymbol{\chi}} = r\left(\frac{p'_{eq}}{p_0}\right)^{\frac{1}{n-1}} \cdot \frac{\partial p_{eq}}{\partial \boldsymbol{\chi}} = \dot{\lambda} \cdot \frac{\partial p'_{eq}}{\partial \boldsymbol{\chi}} \tag{11}$$

Where, $\dot{\lambda}$ serves as a traditional multiplier and in dissipative stress space, the equivalent stress measure is:

$$p'_{eq} = \mathrm{tr}\boldsymbol{\chi}\left(\frac{1}{3} + \frac{\mathrm{tr}\boldsymbol{\sigma}\,\mathrm{tr}\left(\boldsymbol{\sigma}^{-1}\cdot\left({}^{D}\boldsymbol{\chi}\right)^{2}\right)}{\left(\mathrm{tr}\boldsymbol{\chi}\cdot M_{SMP}\right)^{2}}\right)$$
$$^{D}\boldsymbol{\chi} = \boldsymbol{\chi} - \frac{\mathbf{1}}{3}\mathrm{tr}\boldsymbol{\chi} \tag{12}$$

Where **1** is identity tensor. The partial derivative $\partial p^{eq}/\partial\boldsymbol{\chi}$, in true stress, becomes:

$$\frac{\partial p'_{eq}}{\partial\boldsymbol{\chi}} = \frac{\mathbf{1}}{3}\cdot\left(1-\left(\frac{\eta_{SMP}}{M_{SMP}}\right)^{2}\right) - \frac{2p'}{M_{SMP}{}^{2}}\cdot{}^{D}\boldsymbol{\sigma}^{-1}$$
$$^{D}\boldsymbol{\sigma}^{-1} = \boldsymbol{\sigma}^{-1} - \frac{\mathbf{1}}{3}\mathrm{tr}\boldsymbol{\sigma}^{-1} \tag{13}$$

In incremental form eq. (11) become:

$$\Delta\boldsymbol{\varepsilon}^{p} = \Delta\lambda\cdot\frac{\partial p_{eq}}{\partial\boldsymbol{\chi}} \tag{14}$$

Where a multiplier $\Delta\lambda$ is defined. A Taylor expansion of $\Delta\lambda$, when utilizing that the dissipative generalized stress and the true stress are the same, gives:

$$\Delta\lambda = \Delta t\cdot\left(\dot{\lambda} + \left(\frac{\partial\dot{\lambda}}{\partial\boldsymbol{\sigma}} + \frac{\partial\dot{\lambda}}{\partial\boldsymbol{\chi}}\right):\Delta\boldsymbol{\sigma} + \frac{\partial\dot{\lambda}}{\partial p_0}\Delta p_0\right) \tag{15}$$

Since Δp_0 and $\Delta\boldsymbol{\sigma} = \Delta\boldsymbol{\chi}$ depend on $\Delta\boldsymbol{\varepsilon}^{p}$, the equation is expressed in terms of $\Delta\lambda$ as:

$$\Delta\lambda = \frac{nom}{denom}$$
$$nom = \dot{\lambda} + \frac{\partial\dot{\lambda}}{\partial p'_{eq}}\cdot\left(\frac{\partial p'_{eq}}{\partial\boldsymbol{\sigma}} + \frac{\partial p'_{eq}}{\partial\boldsymbol{\chi}}\right):\mathbf{D}\cdot\Delta\boldsymbol{\varepsilon}$$
$$denom = \left\{\begin{array}{l}\dfrac{1}{\Delta t} - \dfrac{\partial\dot{\lambda}}{\partial p_0}\cdot\dfrac{p_0}{\lambda-\kappa}\mathrm{tr}\left(\dfrac{\partial p'_{eq}}{\partial\boldsymbol{\chi}}\right)\\ +\dfrac{\partial\dot{\lambda}}{\partial p'_{eq}}\cdot\left(\dfrac{\partial p'_{eq}}{\partial\boldsymbol{\sigma}} + \dfrac{\partial p'_{eq}}{\partial\boldsymbol{\chi}}\right):\mathbf{D}\cdot\dfrac{\partial p'_{eq}}{\partial\boldsymbol{\chi}}\end{array}\right\} \tag{16}$$

Where, in true stress:

$$\frac{\partial p_{eq}}{\partial\boldsymbol{\sigma}} = \frac{1}{M_{SMP}{}^{2}}\left(\mathbf{1}\cdot\frac{\mathrm{tr}\left(\boldsymbol{\sigma}^{-1}\cdot\left({}^{D}\boldsymbol{\sigma}\right)^{2}\right)}{\mathrm{tr}\boldsymbol{\sigma}} - \boldsymbol{\sigma}^{-1}\cdot\left({}^{D}\boldsymbol{\sigma}\right)^{2}\boldsymbol{\sigma}^{-1}\right)$$
$$^{D}\boldsymbol{\sigma} = \boldsymbol{\sigma} - \frac{\mathbf{1}}{3}\mathrm{tr}\boldsymbol{\sigma} \tag{17}$$

This gives all necessary equation for implementation.

The hypoplastic equations are implemented in a series of MATLAB routines that use a forward Euler integration scheme. A function calculates the objective stress rate based on the actual stress, strain rate and void ratio. The integration and control of the loading conditions—whether strain-controlled, stress-controlled, or mixed—is handled externally via scripts that update the stress state, strain, and state variables accordingly. For general applications, a UMAT implementation of clay hypoplasticity (Mašín, 2014) is available on SoilModels.com (Gudehus, 2008).

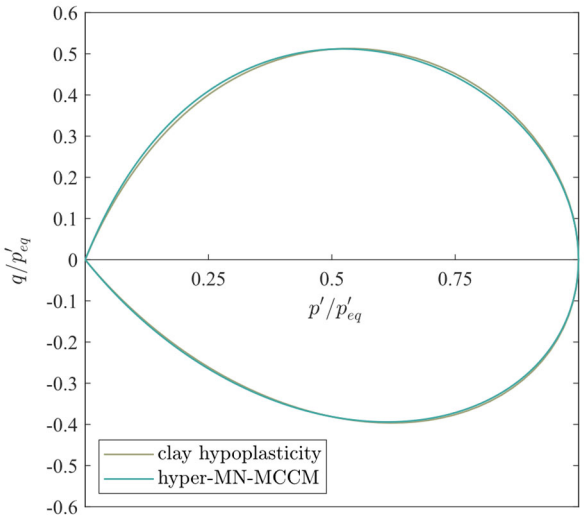

Figure 3. ASBS for clay hypoplasticity and yield surface for hyper-MN-MCCM in the normalized $p' - q$ stress plane

3 CRITICAL STATE PREDICTIONS

Different Over Consolidation Ratios (OCRs) give different amounts of varying dilatancy until critical state is reached. To compare the models the results of different simulations are shown in a normalized deviatoric plane (π-plane) and in the effective mean vs. deviatoric stress ($p' - q$) plane. For the different analyses with MN-MCCM the parameters in Table 1 are used. For the simulations with hypoplasticity the parameters according to Table 2 are used. In this paper the Lode angle for stress and strain is defined such that θ = -π/6 means triaxial compression. θ_σ is used for stress Lode angle and θ_ε for strain Lode angle. Here since all tests are started at isotropic state, strain Lode angle and strain rate Lode angles are equal: $\theta_\varepsilon = \theta_{\dot{\varepsilon}}$.

Table 1. Parameters for MN-MCCM

Parameter	Symbol	Value	Unit
Elastic bulk compressibility parameter	κ	0.010	-
Elastic shear stiffness parameter	g_s	50	-
Critical state parameter	M_{SMP}	0.76	-
Bulk compressibility parameter	λ	0.10	-

Table 2. Parameters for clay hypoplasticity

Parameter	Symbol	Value	Unit
Critical friction angle	φ_c	25	°
Ordinat intercept of NCL	N	1	-
Slope of NCL	λ^*	0.10	-
Slope of unloading and reloading line	κ^*	0.01	-
Controls shear modulus	ν	0.10	-
Controls shape of ASBS	a	0.30 (default)	-

3.1 *At constant volume for different initial OCRs*

Constant volume (undrained) true triaxial simulations of samples at isotopic initial stress at OCR = 1 and OCR = 8 for five different strain Lode angles, θ_ε (in the full interval -π/6 to π/6), are presented here. The simulations are run until 30% of deviatoric strain. For the two models, Figure 4 and Figure 5 show the stress paths in principal stress space (the initial yield surface/ ASBS for the preconsolidation stress is included).

Figure 6 and Figure 7 show the π-plane projections for OCR = 1 and 8 (the initial yield surface / ASBS for OCR=1 included in the back). It is observed that for the MN-MCCM at OCR = 1 the stress paths are twisting towards the 'compression' corner of the MN failure criterion. For OCR = 8 the paths are first going towards 'compression' corner before slightly turning towards 'extension' corner of MN. The elastic region can also be observed at OCR = 8. Note that, since the results are not normalized on the running size of the yield surface the for OCR = 1 curves end up outside the surface and for OCR = 8 end up on the inside. Consistent with the above, simulations with hypoplasticity were carried out for OCR = 1 and OCR = 8. For OCR = 1, the initial stress state lies on the normal compression line ($p'_{ini} = p'_0$, no unloading); for OCR = 8, the samples were unloaded from the NCL to $p'_{ini} = p'_0/8$. The ASBS shown in Figure 7 corresponds to the preloading value p'_0. During undrained loading, the void ratio remains constant, which in hypoplasticity implies constant Hvorslev equivalent pressure $p'_e = p'_0$. As a result, the ASBS at preloading coincides with the p'_e surface, and normally consolidated paths end on the ASBS of the preloading stress p'_0 (Figure 7, top). For OCR = 8, the stress paths remain within the p'_0 surface (Figure 7, below), since p'_e was reduced by unloading due to increase in void ratio, and the current ASBS is therefore smaller.

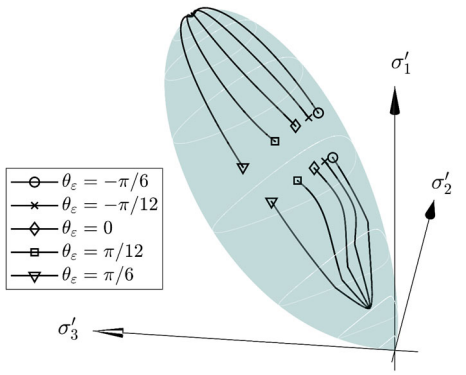

Figure 4. Undrained response of MN-MCCM for *OCR* = 1 and 8 for different strain Lode angles in principal stress space

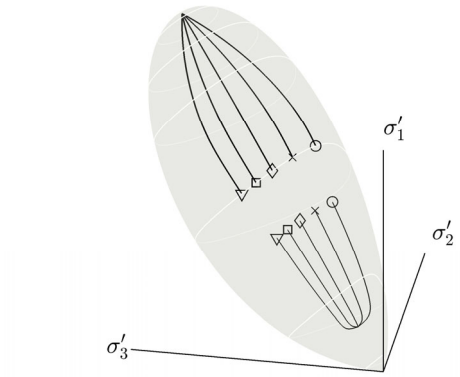

Figure 5. Undrained response of hypoplastic clay model for *OCR* = 1 and 8 for different strain Lode angles in principal stress space

Figure 8 and Figure 9 gives the stress response in normalized $p' - q$ stress plane for MN-MCCM and the hypoplastic clay model respectively. It should be noted that due to that in the hypoplastic clay model there is no split of strain into elastic and plastic strain, the critical state for OCR = 1 is fixed by the initial asymptotic state surface ($p'_{cr}/p_{0ini} = 0.50$). For the MN-MCCM the OCR = 1 and OCR = 8 ends slightly above and slightly below the initial critical state value respectively ($p'_{cr}/p_{0ini} \neq 0.5$). Consequently, for OCR = 8 hypoplasticity will also give lower critical state value than MN-MCCM.

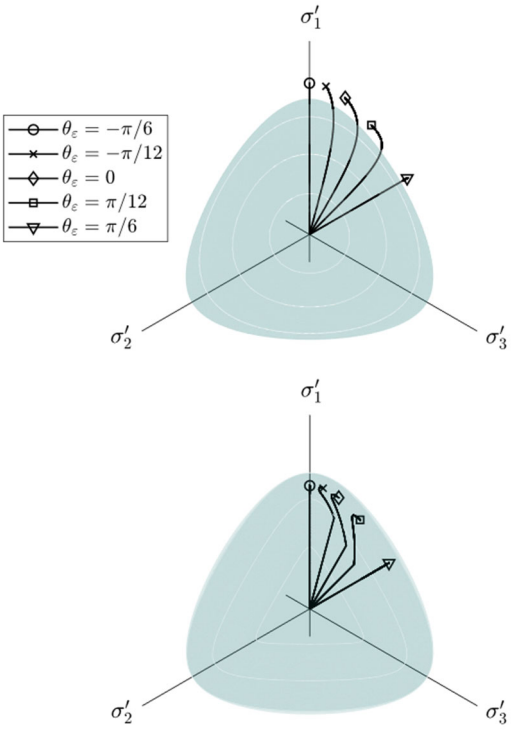

Figure 6. Undrained response of MN-MCCM for *OCR* = 1 (top) and 8 (bottom) for different strain Lode angles in the π-plane

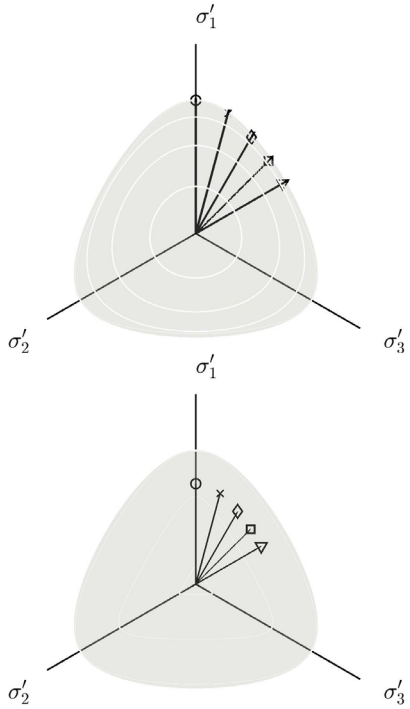

Figure 7. Undrained response of hypoplastic clay model for *OCR* = 1 (top) and 8 (bottom) for different strain Lode angles in the π-plane

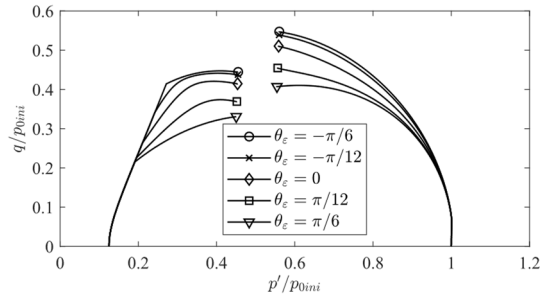

Figure 8. Undrained response of MN-MCCM for *OCR* = 1 and 8 for different strain Lode angles in the normalized *p'-q* stress space

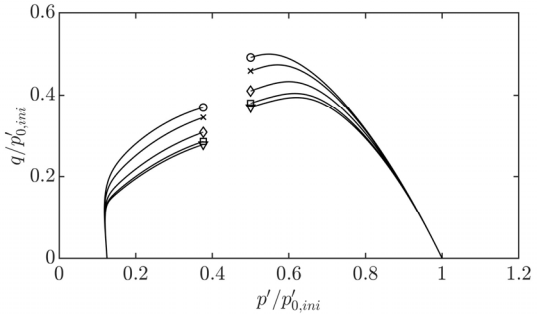

Figure 9. Undrained response of hypoplastic clay model for *OCR* = 1 and 8 for different strain Lode angles in the normalized *p'-q* stress space

3.2 *At constant p´ for different initial OCRs*

Results of simulation of shearing to 100% of deviatoric strain at constant mean effective stress are presented in π-plane below. Figure 10 and Figure 11 gives results with MN-MCCM and the hypoplastic clay model for OCR = 1, 2 and 8 at top, middle and bottom, respectively. For clarity, the final and 'initial' MN-yield surfaces are included. The plots show the tendency of the MN-MCCM to 'drift' towards the 'compression' corner, meaning that the stress Lode angles are less than the strain Lode angles ($\theta_\sigma < \theta_\varepsilon$). The 'drift' increases with increasing friction mobilization. This is qualitatively in-line with the discrete element simulations of isochoric plane strain compression tests, where a strain Lode angle $\theta_\varepsilon = 0$ was prescribed and a stress Lode angle $\theta_\sigma < 0$ was observed at critical state for varying friction (Medicus et al., 2024, Figure 12). Further, for OCR = 2 and 8 the elastic region is observed. For OCR = 8 the softening (dilation) is observed by the reduction in deviatoric stress. It is also observed that the drift towards the 'compression' corner reduces with reducing mobilized friction. For the hypoplastic model the stress paths are again straight towards the asymptotic state for OCR = 1 and 2 for an initially hydrostatic consolidated sample. For OCR = 8 the paths are straight out and in again, but the path returns at a lower mobilized friction than the MN-MCCM. The critical stress surface is included for OCR=1 and 2; for OCR = 8, both the critical surface and the assumed peak envelope are shown. Peak states for OCR = 8 reach Matsuoka–Nakai equivalent mobilized friction angles between 42.8° (triaxial compression) and 43.4° (triaxial extension); the peak envelope is plotted for 43.1°.

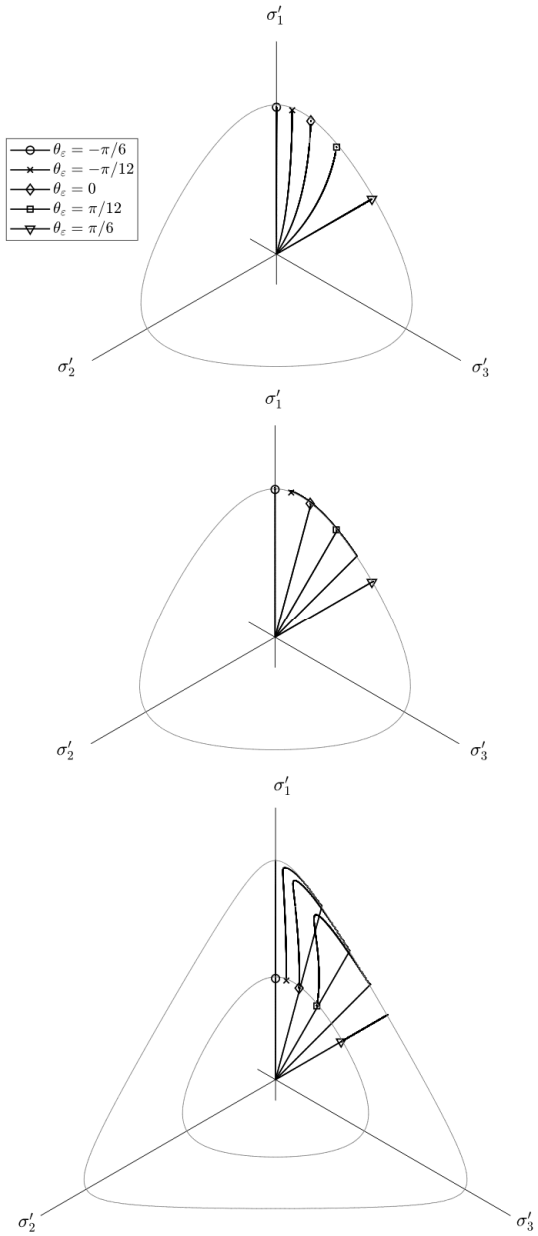

Figure 10. Response at constant p' of MN-MCCM for *OCR* = 1 (top), 2 (middle) and 8 (bottom) for different strain Lode angles in the π-plane

4 CONCLUSIONS

The intention of the work presented was to demonstrate similarities and differences between the performance of the MN-MCCM, developed under the framework of hyperplasticity, and the hypoplastic clay model. It is shown that the yield surface of the MN-MCCM model and the ASBS of clay hypoplasticity is qualitatively very similar. The number of parameters for the two models is also comparable. In terms of stress paths to critical state at constant volume and at constant mean effective stress the models are different. In the π-plane the stress paths for clay hypoplasticity follows directly the strain Lode angle for initially hydrostatic stress state. While, in the hyperplastic MN-MCCM the stress paths for OCR = 1 deviates towards the 'compression' corner. This deviation towards the 'compression' corner ($\theta_\sigma < \theta_\varepsilon$) is also supported by DEM studies (Medicus et al., 2024).

The peak friction reached at constant mean effective stress for OCR = 8 is higher in MN-MCCM than in hypoplasticity. This is mainly due to the pure elasticity inside yield for MN-

MCCM. Further, when the response of MN-MCCM is compared to that of hypoplasticity, the split in elastic and plastic strains in MN-MCCM also explains some of the differences in the effective stress paths, induced by plastic dilation, in the undrained (constant volume) simulations. For OCR = 8 it is observed that for MN-MCCM the drift is first towards the 'compression' corner, but as dilation is reduced the paths turn (drift back in direction of extension corner). However, still, the critical state value of the stress Lode angle stays less than the strain Lode angle imposed under shearing.

To have a better basis to evaluate the performance of the models compared to clay behavior, results of true triaxial test on reconstituted and natural clays should be used for comparison.

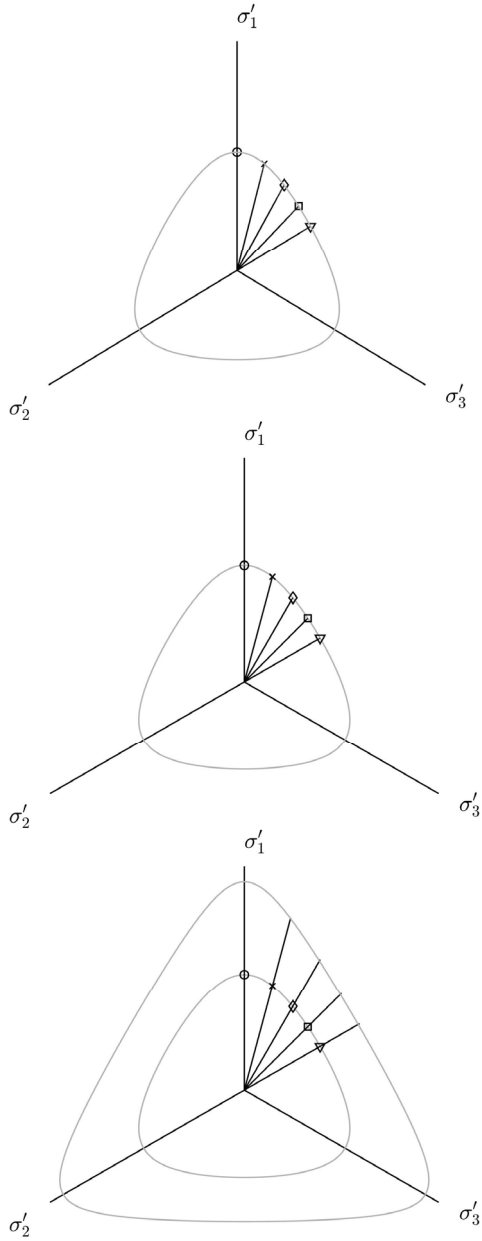

Figure 11. Response at constant p' of hypoplastic clay model $OCR = 1$ (top), 2 (middle) and 8 (bottom) for different strain Lode angles in the π-plane

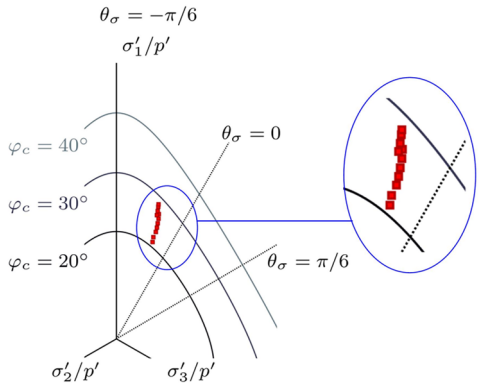

Figure 12. Critical stress states of DEM simulations of isochoric plane-strain compression tests (red squares) with varying friction; the endpoints of each simulation are shown. Figure modified from Medicus et al. (2024)

5 ACKNOWLEDGEMENTS

This research was funded in part by the Austrian Science Fund (FWF) 10.55776/V918. G.M. is funded by the FWF. For open access purposes, the author has applied a CC BY public copyright license to any author accepted manuscript version arising from this submission.

6 REFERENCES

Dadras-Ajirlou, D., Grimstad, G., Ali Ghoreishian Amiri, S. & Nordal, S. 2023. A set of hyper-viscoplastic critical state models with different friction mobilisation criteria. *International Journal of Solids and Structures,* 273**,** 112267.

Gudehus, G., Amorosi, A., Gens, A., Herle, I., Kolymbas, D., Mašín, D., Muir Wood, D., Nova, R., Niemunis, A., Pastor, M., Tamagnini, C. & Viggiani, G. 2008. The soilmodels.info project. *International Journal for Numerical and Analytical Methods in Geomechanics*, 32, 1571-1572

Houlsby, G. T., Amorosi, A. & Rojas, E. 2005. Elastic moduli of soils dependent on pressure: a hyperelastic formulation. 55**,** 383-392.

Houlsby, G. T. & Puzrin, A. M. 2006. *Principles of hyperplasticity: an approach to plasticity theory based on thermodynamic principles*, Springer Science & Business Media.

Kadlíček, T.; Janda, T.; Šejnoha, M.; Mašín, D.; Najser, J.; Beneš, Š. 2022. Automated calibration of advanced soil constitutive models. Part II: hypoplastic clay and modified Cam-Clay. *Acta Geotechnica*, 17, 3439–3462.

Kolymbas, D. 1977. A rate-dependent constitutive equation for soils. *Mechanics Research Communications,* 4**,** 367-372.

Mašín, D. 201s3. Clay hypoplasticity with explicitly defined asymptotic states. *Acta Geotechnica,* 8**,** 481-496.

Mašín, D. 2014. Clay hypoplasticity model including stiffness anisotropy. *Géotechnique*, 64, 232-238.

Matsuoka, H. & Nakai, T. Stress-deformation and strength characteristics of soil under three different principal stresses. Proceedings of JSCE, 1974. 59–70.

Medicus, G., Pouragha, M., Ostermann, A. & Fellin, W. 2024. On the friction dependency of the stress Lode angle. *International Journal for Numerical and Analytical Methods in Geomechanics,* 48**,** 1001-1017.

Roscoe, K. H. & Burland, J. B. 1968. On the generalized stress–strain behaviour of wet clay. Engineering Plasticity, 1968. Cambridge, 535-609.

Schofield, A. & Wroth, P. 1968. *Critical state soil mechanics,* New York, McGraw-Hill.

Wu, W. & Kolymbas, D. 2000. Hypoplasticity then and now. *In:* Kolymbas, D. (ed.) *Constitutive Modelling of Granular Materials.* Berlin, Heidelberg: Springer Berlin Heidelberg.

Ziegler, H. 1983. *An Introduction to Thermomechanics*, North-Holland.